Journal of Marine Science and Application (2026) 25: 702-712
https://doi.org/10.1007/s11804-026-00811-y

RESEARCH ARTICLE

Real-time Estimation of Instantaneous Speed in Diesel Engines Based on the Extended Kalman Filter

Zhongxin Shi[1], Hongzi Fei[1], Liuping Wang[2], Bingxin Liu[1] and Yilin Liu[1]

Received: 13 April 2025 / Accepted: 04 September 2025

Abstract
The instantaneous speed of diesel engines contains an abundance of information, regarding fuel supply stability and individual cylinder performance. Real-time acquisition of accurate instantaneous speed is crucial for monitoring cylinder-to-cylinder uniformity, diagnosing faults, and enabling precise speed control in marine diesel engines. However, measurement noise distorts the signal, which makes it significantly difficult to monitor the effective information in the actual operation. To address this challenge, this paper proposes a novel real-time filtering method using an extended Kalman filter (EKF). According to the characteristics of crankshaft instantaneous speed of diesel engine, a dedicated state-space model is derived. The EKF utilizes the model to perform real-time feedback and rolling optimization effectively suppressing noise. The performance of the method proposed is validated using both simulated signals and experimental data from a four-cylinder marine diesel engine. Simulation and experimental results demonstrate that the coefficient of determination R^2 between the estimated and actual speed reaches 99.83%, while the signal-to-noise ratio (SNR) improves by above 10% on average across different operating conditions. This enhancement enables reliable real-time engine state monitoring and control.

Keywords Marine diesel engine; Crankshaft instantaneous speed; State-space model; Extended kalman filter; Real-time estimation; Noise filtering

1 Introduction

The actual instantaneous speed of marine diesel engines exhibits significant fluctuation due to multi-cylinder combustion dynamics (Qiao and Gu, 2019; Kazienko and Chybowski, 2020). The instantaneous speed of the crankshaft directly reflects the combustion dynamics in each cylinder. These microscopic fluctuations are closely related to critical cylinder events, such as fuel injection timing, in-cylinder pressure, and mechanical status. The information is often obscured in global measurements such as power and fuel rate (Lin et al., 2015; Xi et al., 2016; Qian et al., 2022). Therefore, instantaneous speed analysis is crucial for maintaining optimal performance and health monitoring (Chang and Hu, 2010; Zhang et al., 2019; Zhao and Chen, 2019). By using the instantaneous speed to extract suitable characteristic parameters, researchers have realized the diagnosis of valve leakage, ignition anomalies and cylinder non-uniformity (Lin et al., 2015; Zhao et al., 2015). Nevertheless, the accurate measurement of instantaneous speed is severely compromised by noise contamination from mechanical vibrations, sensor inaccuracies, and data acquisition limitations (Liu et al., 2022; Liu et al., 2024). Pan and Zhang (2011) proposed a method of combining an enhanced differential rank pulse detector with a Butterworth low-pass filter to effectively suppress impulse noise. However, its complex threshold tuning and fixed cutoff frequency limit adaptability across varying operating conditions. Yang et al. (2018) leveraged the Hilbert-Huang Transform (HHT) involving Empirical Mode Decomposi-

Article Highlights

- A novel nonlinear state-space model for crankshaft instantaneous speed is proposed, using speed fluctuation, its derivative, and average speed as states, avoiding complex physical modeling.
- An Extended Kalman Filter (EKF) is designed for real-time estimation, effectively suppressing noise while maintaining fast tracking of speed dynamics.
- The proposed EKF-based method is tested with a variable-speed simulation signal, demonstrating robust noise suppression and accurate tracking with a coefficient of determination R^2 of 0.998 3 against the noise-free signal.
- The method is applied to a 4-cylinder marine diesel engine across various operating conditions. Results confirm its practical effectiveness, showing a significant SNR improvement over 10% on average in real-time.

✉ Hongzi Fei
fhz@hrbeu.edu.cn

[1] College of power and Energy Engineering, Harbin Engineering University, Harbin 150001, China

[2] School of Engineering, RMIT University, VIC 3000, Australia

tion (EMD), spectral analysis, and adaptive Butterworth filter. Although EMD and Butterworth filter are adaptive, its computational intensity necessitates offline processing, hindering real-time engineering applications.

Beyond real-time control, accurate instantaneous speed estimation is crucial for effective predictive maintenance strategies (Xie et al., 2023; Kai et al., 2023). The microscopic variations of the crankshaft instantaneous speed signal can serve as early fault indicators, such as injector blockage, minor valve leakage, uneven cylinder compression or bearing wear (Kazienko and Chybowski, 2020; Chang and Hu, 2010). If these initial faults are not detected, they will lead to reduced efficiency, increased emission, or severe damage. Real-time instantaneous speed signal can continuously monitor the diagnostic characteristics, enabling the timely detection of anomalies before they develop into significant issues.

Therefore, achieving high-performance closed-loop speed control and real-time health monitoring critically requires accurate instantaneous speed signals. This necessitates that the filtering method satisfies three core requirements: high noise suppression capability, computational efficiency for recursive processing, and strict real-time performance.

The extended Kalman filter (EKF) serves as a real-time recursive estimator that effectively addresses nonlinear dynamics and measurement uncertainty through linearizing Jacobian matrix at each sampling point (Wang and Guan, 2022). Different from the offline methods, the EKF operates recursively, using only the current measurement and prior state estimation. By incorporating process and measurement covariance matrices, it suppresses noise and achieves optimal estimation through adaptive feedback correction (Rana et al., 2019; Meng et al., 2023). Cao et al. (2021) and Zerdali (2019) have successfully applied the EKF for real-time tuning control and adaptive estimation of target variables. Furthermore, EKF is widely adopted in engine parameter estimation. For instance, Kallenberger et al. (2007) applied EKF and UKF for cylinder-wise torque estimation by fusing dual speed signals and cylinder pressure data, while Quartullo et al. (2023) reconstructed in-cylinder pressure from speed measurements using an experimental combustion model. However, existing methods focus on torque or pressure reconstruction, often requiring additional sensors or complex physical models. Crucially, the real-time denoising of instantaneous speed signals is a gap critical for closed-loop control and fault diagnosis.

This paper aims to optimally filter the speed signal in real time based on the EKF. An accurate model is required for the EKF design. However, it is challenging to establish a physical motion model based on the dynamic equation due to the complex structure of diesel crankshaft (Wu et al., 2021; Yu and Duan, 2014).

To realize real-time filtering and state monitoring of the instantaneous speed, we establish a phenomenological model based on the instantaneous speed fluctuation law. Specifically, a novel state-space model is proposed which takes the fluctuation of the instantaneous speed, the derivative of the fluctuation and the average rotational speed as the state variables. On this basis, the EKF for the real-time filtering estimation of the speed signal is designed and studied.

2 Modeling of instantaneous speed of diesel engines

The successful application of the extended Kalman filter (EKF) for real-time filtering hinges on establishing an accurate instantaneous speed model. This section derives a nonlinear speed model based on the instantaneous speed characteristics. Subsequently, a nonlinear state-space model incorporating three state variables is formulated, and the observability of the model is verified.

2.1 Analysis of instantaneous speed characteristics of diesel engine

During the actual operation of the diesel engines, the speed dose not remain at a fixed value. It will fluctuate around the target speed, as a result of each cylinder in turn burning and driving the crankshaft. Based on these characteristics, the instantaneous speed can be approximated as a periodic sinusoidal signal (Zheng et al., 2017). In this paper, a four-stroke diesel engine is used as the standard to construct the model. The modeling assumption in this paper ignores the small effects such as torsional vibration and irregular combustion, and the instantaneous speed fluctuation is almost driven by cylinder ignition. The instantaneous speed signal of the engines is approximated as the sum of the average speed and the speed fluctuation:

$$n = \bar{n} + a\sin(\omega t) \tag{1}$$

where $\bar{n}$ denotes the average speed, a represents the amplitude of the speed fluctuation, ω is the angular frequency corresponding to speed.

Based on the structural information of the diesel engines, the angular frequency is derived as:

$$\omega = 2\pi f \tag{2}$$

where f denotes the fundamental frequency of the speed.

For a four-stroke multi-cylinder diesel engine with cylinder number I, each working cycle consists of two crankshaft rotations, during which the number of firings is I. Thus, the number of firings per crankshaft rotation is $I/2$. Then the fundamental frequency f is derived from the average speed as:

$$f = \frac{I}{2} f_c = \frac{I}{2}\frac{\bar{n}}{60} \tag{3}$$

where f_c is the crankshaft rotational frequency.

Therefore, the relationship between the angular frequency corresponding to speed and average speed can be summarized in the equation (4):

$$\omega = 2\pi \frac{I}{2} \frac{\bar{n}}{60} = \frac{\pi I}{60} \bar{n} = b\bar{n} \tag{4}$$

where b is defined as a constant here.

2.2 State space model of instantaneous speed

To design the EKF, an accurate state-space model of the rotational speed must be established. The core challenge lies in selecting state variables that ensure model observability while capturing essential dynamics. Since instantaneous speed estimation requires tracking of speed fluctuations, the state variable is constructed as follows:

$$\boldsymbol{x} = \begin{bmatrix} x_1 \\ x_2 \\ x_3 \end{bmatrix} = \begin{bmatrix} a\sin(\omega t) \\ a\cos(\omega t) \\ \bar{n} \end{bmatrix} \tag{5}$$

where, x_1 denotes the fluctuation of the instantaneous speed, x_2 represents the derivative of the fluctuation, and x_3 is the average rotational speed.

Under steady conditions, the average rotational speed remains constant. Then equation (5) is derived as:

$$\begin{cases} \dot{x}_1 = \dfrac{\mathrm{d}x_1}{\mathrm{d}t} = a\omega\cos(\omega t) = x_3 x_2 \\ \dot{x}_2 = \dfrac{\mathrm{d}x_2}{\mathrm{d}t} = -a\omega\sin(\omega t) = -x_3 x_1 \\ \dot{x}_3 = \dfrac{\mathrm{d}x_3}{\mathrm{d}t} = 0 \end{cases} \tag{6}$$

According to the equations (1) and (6), the nonlinear continuous time state-space model of the instantaneous speed is derived as the equation (7):

$$\begin{cases} \dot{\boldsymbol{x}} = \begin{bmatrix} \dot{x}_1 \\ \dot{x}_2 \\ \dot{x}_3 \end{bmatrix} = \begin{bmatrix} \omega x_2 \\ -\omega x_1 \\ 0 \end{bmatrix} = \begin{bmatrix} f_1(\boldsymbol{x}) \\ f_2(\boldsymbol{x}) \\ f_3(\boldsymbol{x}) \end{bmatrix} = \boldsymbol{f}(\boldsymbol{x}) \\ \boldsymbol{y} = C\boldsymbol{x} = \begin{bmatrix} 1 & 0 & 1 \end{bmatrix} \begin{bmatrix} x_1 \\ x_2 \\ x_3 \end{bmatrix} = x_1 + x_3 \end{cases} \tag{7}$$

Where $\boldsymbol{y}$ is the instantaneous speed output of the system.

2.3 Observability verification of instantaneous speed state space equation

Furthermore, to rigorously verify the observability of the nonlinear system, Lie derivative analysis is performed. According to the output function in equation (7), the Lie derivatives are computed as:

$$\begin{cases} L_f^0 h = \boldsymbol{y}(x) = x_1 + x_3 \\ L_f h = \dfrac{\partial \boldsymbol{y}}{\partial \boldsymbol{x}} \boldsymbol{f}(x) = \begin{bmatrix} 1 & 0 & 1 \end{bmatrix} \begin{bmatrix} \omega x_2 \\ -\omega x_1 \\ 0 \end{bmatrix} = \omega x_2 \\ L_f^2 h = \dfrac{\partial (L_f h)}{\partial \boldsymbol{x}} \boldsymbol{f}(x) = \begin{bmatrix} 0 & \omega & 0 \end{bmatrix} \begin{bmatrix} \omega x_2 \\ -\omega x_1 \\ 0 \end{bmatrix} = -\omega^2 x_1 \end{cases} \tag{8}$$

Then the observability matrix $\mathcal{O}$ is formed by the gradients:

$$\mathcal{O} = \begin{bmatrix} \nabla L_f^0 h \\ \nabla L_f h \\ \nabla L_f^2 h \end{bmatrix} = \begin{bmatrix} 1 & 0 & 1 \\ 0 & \omega & 0 \\ -\omega^2 & 0 & 0 \end{bmatrix} \tag{9}$$

The determinant of the equation (9) is:

$$\det(\mathcal{O}) = \omega^3 \tag{10}$$

The system is locally observable when $\det(\mathcal{O}) \neq 0$, which requires:

$$\omega \neq 0 : b \neq 0, x_3 \neq 0 \tag{11}$$

Since x_3 is the average speed and $b = \pi I/60 > 0$, the limitations are always satisfied when the diesel engine is running, which confirms that the nonlinear system is observable.

3 Design of extended kalman filter

To mitigate noise and achieve real-time filtering, an instantaneous speed extended Kalman filter (EKF) is designed based on the equation (7). This section details the discretization and linearization of the nonlinear state-space model, followed by a comprehensive derivation of the EKF-based instantaneous speed estimation procedure.

3.1 Discretized instantaneous speed state space equation

Assuming that the sampling interval is Δt, by discretizing the state-space model of the equation (7), the derivative of the state variable $\boldsymbol{x}$ at time t_{k-1} can be approximated as:

$$\dot{\boldsymbol{x}}(t_{k-1}) = \boldsymbol{f}\left(\boldsymbol{x}(t_{k-1})\right) = \frac{\boldsymbol{x}(t_k) - \boldsymbol{x}(t_{k-1})}{\Delta t} \tag{12}$$

where $k = 1, 2, \cdots, t_k = k \cdot \Delta t$.

Equation (12) is converted into:

$$\boldsymbol{x}\left(t_k\right) = \boldsymbol{x}\left(t_{k-1}\right) + \Delta t\boldsymbol{f}\left(\boldsymbol{x}\left(t_{k-1}\right)\right) \tag{13}$$

Replace t_k t_{k-1} with k $k-1$, then the equation (13) is transformed into:

$$\boldsymbol{x}(k) = \boldsymbol{x}(k-1) + \Delta t\boldsymbol{f}\left(\boldsymbol{x}(k-1)\right) \tag{14}$$

where $\boldsymbol{f}\left(\boldsymbol{x}(k-1)\right)$ is as follows:

$$\boldsymbol{f}\left(\boldsymbol{x}(k-1)\right) = \begin{bmatrix} f_1\left(\boldsymbol{x}(k-1)\right) \\ f_2\left(\boldsymbol{x}(k-1)\right) \\ f_3\left(\boldsymbol{x}(k-1)\right) \end{bmatrix} = \begin{bmatrix} \omega(k-1)x_2(k-1) \\ -\omega(k-1)x_1(k-1) \\ 0 \end{bmatrix} \tag{15}$$

At this point, the discretized state-space equation is obtained as shown in the equation (16):

$$\begin{cases} \boldsymbol{x}(k) = \boldsymbol{x}(k-1) + \Delta t\boldsymbol{f}\left(\boldsymbol{x}(k-1)\right) \\ \boldsymbol{y}(k) = \boldsymbol{C}\boldsymbol{x}(k) \end{cases} \tag{16}$$

Incorporating process noise $\boldsymbol{w}(k)$ and measurement noise $\boldsymbol{v}(k)$, the equation (16) becomes:

$$\begin{cases} \boldsymbol{x}(k) = \boldsymbol{x}(k-1) + \Delta t\cdot\boldsymbol{f}\left(\boldsymbol{x}(k-1), \boldsymbol{w}(k-1)\right) = \\ \qquad \boldsymbol{g}\left(\boldsymbol{x}(k-1), \boldsymbol{w}(k-1)\right) \\ \boldsymbol{y}(k) = \boldsymbol{C}\boldsymbol{x}(k) + \boldsymbol{v}(k-1) \end{cases} \tag{17}$$

where $\boldsymbol{w}(k)$ and $\boldsymbol{v}(k)$ are independent zero-mean Gaussian white noise, and their covariance matrices are $\boldsymbol{Q}$ and $\boldsymbol{R}$, respectively. $\boldsymbol{Q}$ is a diagonal matrix, $\boldsymbol{Q} = \mathrm{diag}\left(q_1, q_2, q_3\right)$.

3.2 Linearization of state space equations

The first step of the extended Kalman filter is to linearize the model by calculating the Jacobian matrices at each sampling instant. Let $\hat{x}(k)^-$ denote the priori estimate and $\hat{x}(k)^+$ present the posteriori estimate.

If $\boldsymbol{x}(k-1)_0 = \hat{x}(k-1)^+, \boldsymbol{w}(k-1)_0 = 0$, then the first order Taylor series expansion of the nonlinear function at $\left(\boldsymbol{x}(k-1)_0, \boldsymbol{w}(k-1)_0\right)$ gives the following approximate linearized expression of the state equation:

$$\begin{aligned} \boldsymbol{x}(k) = \boldsymbol{g}\left(\boldsymbol{x}(k-1), \boldsymbol{w}(k-1)\right) \approx \\ \boldsymbol{g}\left(\hat{\boldsymbol{x}}(k-1)^+, 0\right) + \boldsymbol{M}(k-1)\boldsymbol{w}(k-1) + \\ \boldsymbol{A}(k-1)\left(\boldsymbol{x}(k-1) - \hat{\boldsymbol{x}}(k-1)^+\right) \end{aligned} \tag{18}$$

where $\boldsymbol{A}(k-1)$ and $\boldsymbol{M}(k-1)$ are the Jacobian matrices at $\boldsymbol{x}(k-1)_0 = \hat{\boldsymbol{x}}(k-1)^+, \boldsymbol{w}(k-1)_0 = 0$. From equation (18), they are derived as:

$$\boldsymbol{A}(k-1) = \left.\begin{bmatrix} \frac{\partial g_1}{\partial x_1} & \frac{\partial g_1}{\partial x_2} & \frac{\partial g_1}{\partial x_3} \\ \frac{\partial g_2}{\partial x_1} & \frac{\partial g_2}{\partial x_2} & \frac{\partial g_2}{\partial x_3} \\ \frac{\partial g_3}{\partial x_1} & \frac{\partial g_3}{\partial x_2} & \frac{\partial g_3}{\partial x_3} \end{bmatrix}\right|_{\left(\hat{x}(k-1)^+, 0\right)} = \left.\begin{bmatrix} 1 & \Delta tbx_3 & \Delta tbx_2 \\ -\Delta tbx_3 & 1 & -\Delta tbx_1 \\ 0 & 0 & 1 \end{bmatrix}\right|_{\left(\hat{x}(k-1)^+, 0\right)} \tag{19}$$

$$\boldsymbol{M}(k-1) = \begin{bmatrix} 1 & 0 & 0 \\ 0 & 1 & 0 \\ 0 & 0 & 1 \end{bmatrix} \tag{20}$$

At any sampling instant, $\boldsymbol{M}(k)$ is invariant. Hereafter abbreviated as $\boldsymbol{M}$.

3.3 Estimation of instantaneous speed based on EKF

The EKF algorithm mainly comprises the time update and the measurement update. After initializing $\hat{x}(0)^+$, $P(0)^+$, and selecting appropriate $\boldsymbol{Q}$, $\boldsymbol{R}$, the following steps are iterated at each sampling instant k for optimal state estimation:

The time update phase:

① Compute the priori estimate of the state according to the nonlinear equation (17).

$$\hat{x}(k)^- = \hat{\boldsymbol{x}}(k-1)^+ + \Delta t\left(\boldsymbol{f}\left(\hat{\boldsymbol{x}}(k-1)^+\right) + \boldsymbol{w}(k-1)\right) \tag{21}$$

② Compute the Jacobian matrices at this time according to the equations (19) and (20).

③ Compute the priori estimate of the covariance matrix:

$$\boldsymbol{P}(k)^- = \boldsymbol{A}(k-1)\boldsymbol{P}(k-1)^+\boldsymbol{A}(k-1)^{\mathrm{T}} + \boldsymbol{MQM}^{\mathrm{T}} \tag{22}$$

The measurement update phase:

④ Calculate the Kalman filter gain $\boldsymbol{K}(k)$:

$$\boldsymbol{K}(k) = \boldsymbol{P}(k)^-\boldsymbol{C}^{\mathrm{T}}\left[\boldsymbol{CP}(k)^-\boldsymbol{C}^{\mathrm{T}} + \boldsymbol{R}\right]^{-1} \tag{23}$$

⑤ Calculate the posteriori estimate of the state by using the difference between the instantaneous speed measurement and the prior state estimate for feedback correction.

$$\hat{\boldsymbol{x}}(k)^+ = \hat{\boldsymbol{x}}(k)^- + \boldsymbol{K}(k)\left(\boldsymbol{y}(k) - \boldsymbol{C}\hat{\boldsymbol{x}}(k)^-\right) \tag{24}$$

⑥ Calculate the posteriori estimate of the covariance matrix:

$$\boldsymbol{P}(k)^{+} = \left(\boldsymbol{I} - \boldsymbol{K}(k)\boldsymbol{C}\right)\boldsymbol{P}(k)^{-}\left(\boldsymbol{I} - \boldsymbol{K}(k)\boldsymbol{C}\right)^{\mathrm{T}} + \boldsymbol{K}(k)\boldsymbol{R}\boldsymbol{K}^{\mathrm{T}}(k) \tag{25}$$

Figure 1 shows the process of estimating the diesel engine instantaneous speed signal based on the EKF algorithm.

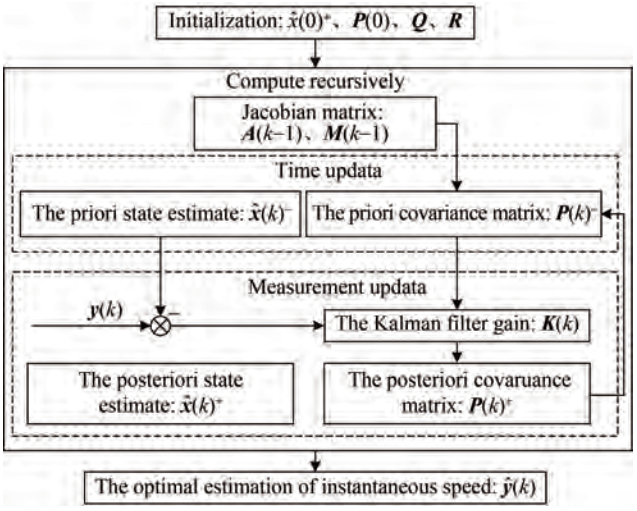

Figure 1 Estimation process of instantaneous speed based on EKF

4 Analysis of simulation signal

4.1 Construction of simulation signal

To validate the estimation performance and assess its general applicability, we construct a simulated instantaneous speed signal for a four-cylinder diesel engine under variable-speed conditions. The signal comprises three distinct stages $S_1 - S_2 - S_3$, each spanning 0.1 seconds.

S_1 runs stably at an average speed of 900 r/min. According to the equation (3), the frequency of S_1 is $F_{S_1} = 30$ Hz. In addition, the amplitude of the fluctuation a will vary for different diesel engines, here the amplitude a of S_1 is set to 20. According to the equation (1), the simulated instantaneous speed of stages S_1 is obtained as follows:

$$y_{S_1}(t) = \bar{y}_{S_1} + a\sin\left(2\pi F_{S_1} t\right) = 900 + 20 \times \sin(2\pi \times 30 \times t) \quad t \in (0, 0.1] \tag{26}$$

Analogously, S_3 runs stably at an average speed of 1 050 r/min. And its frequency is $F_{S_1} = 30$ Hz. Since the speed fluctuation amplitude will decrease with the increase of the average speed, the amplitude S_3 is a quarter of a. And then the expression of stage S_3 is:

$$y_{S_3}(t) = \bar{y}_{S_3} + \frac{1}{4} \times a\sin\left(2\pi F_{S_3} t\right) = 1\,050 + 5 \times \sin(2\pi \times 35 \times t) \quad t \in (0.2, 0.3] \tag{27}$$

In S_2 stage, the speed accelerates linearly from 900 r/min to 1 050 r/min. The amplitude is also set to a quarter of a.

$$y_{S_2}(t) = \bar{y}_{S_1} + \frac{1}{4} \times a\sin\left(2\pi f_{S_1} t\right) + \frac{\left(F_{S_3} - F_{S_1}\right)}{(0.2 - 0.1)} \times \frac{60}{(M/2)} \times (t - 0.1) = 900 + 50 \times 30 \times (t - 0.1) + 5 \times \sin(2\pi \times 30 \times t) \quad t \in (0.1, 0.2] \tag{28}$$

The true signal $y_0(t)$ is formed by combining signals of the three stages:

$$y_0(t) = y_{S_1}(t) + y_{S_2}(t) + y_{S_3}(t) \tag{29}$$

To simulate experimental noise, a random zero-mean white noise $n(t)$ with the amplitude of 3 is added here. The simulation signal $y(t)$ with noise is obtained:

$$y(t) = y_{S_1}(t) + y_{S_2}(t) + y_{S_3}(t) + n(t) \tag{30}$$

The sampling frequency is set to 3 000 Hz. The signal duration is 0.3 s, then the length of the signal N is 900. The simulated signal $y(t)$ is shown in Figure 2.

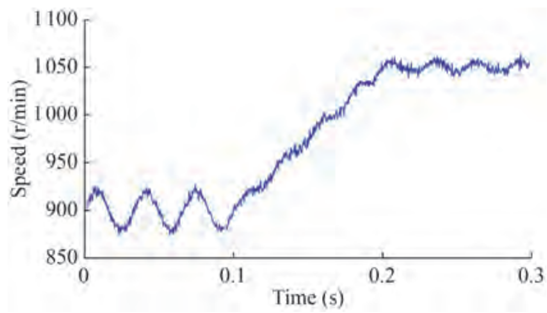

Figure 2 The simulated signal

It can be seen from Figure 2 The simulated signal that the simulated signal contains three stages to simulate the instantaneous speed of the actual measured. We will further analyze the signal in the following chapters.

4.2 Optimization of *Q* and *R* matrix parameters in EKF

In EKF-based instantaneous speed estimation, the process noise covariance $\boldsymbol{Q}$ and measurement noise covariance $\boldsymbol{R}$ critically govern estimation performance, balancing noise suppression against state convergence rate. The value of $\boldsymbol{R}$ reflects the filtering intensity. The $\boldsymbol{R}$ is mainly discussed here with fixed $\boldsymbol{Q} = \mathrm{diag}(0.1, 0.01, 10)$. When $\boldsymbol{R}$ = 30, 40, 50 is selected respectively, the speed is processed, and the results are shown in Figure 3.

It can be seen from Figure 3(a) that the tracking effect of the speed estimation is excellent under variable speed

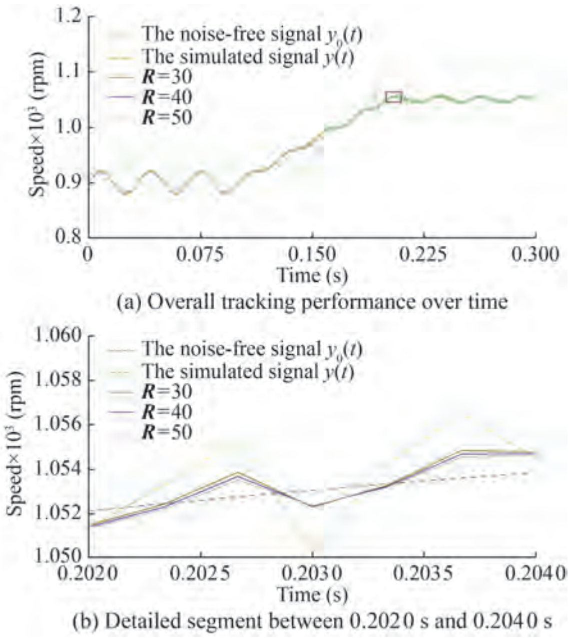

Figure 3 Comparison of instantaneous speed estimation results under different measurement noise covariance $\boldsymbol{R}$

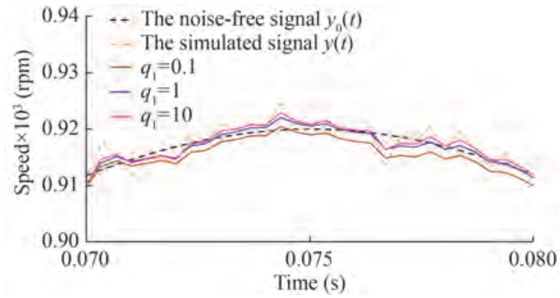

Figure 4 Estimation results of different q_1 at 0.07–0.08 s

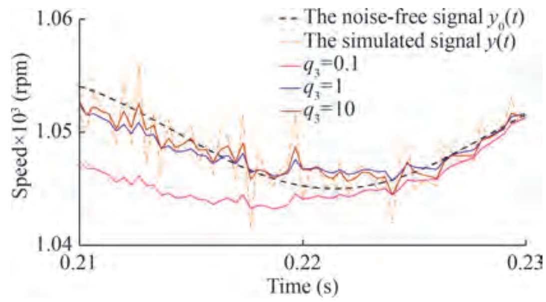

Figure 5 Estimation results of different q_3 at 0.21–0.23s

conditions. The main reason why the varying operating conditions in the middle rising section can also track stably is the flexibility of the noise covariance matrices and the tolerance of the EKF feedback mechanism.

As shown in Figure 3(b), as $\boldsymbol{R}$ gradually increases, the filtering effect on instantaneous speed becomes more obvious. However, the filtering effect does not change significantly when the value of $\boldsymbol{R}$ increases from 40 to 50. To sum up, $\boldsymbol{R}$ = 40 is selected as the optimal measurement noise covariance matrix.

$\boldsymbol{Q}$ is set as a diagonal matrix. The diagonal elements are defined as q_1, q_2 and q_3, corresponding to the process noise intensities of the three state variables. Since the primary objective of the EKF is instantaneous speed filtering, this paper focuses on optimizing q_1 and q_3, while assigning q_2 = 0.01 due to reduced tracking requirements for state variable x_2.

Firstly, the influence of q_1 on the filtering performance is studied. Here, $\boldsymbol{R}$ = 40, q_2 = 0.01 and q_3 = 10 in matrix $\boldsymbol{Q}$ is fixed, and the instantaneous speed estimation results with q_1 = 0.1, 1, 10 respectively were shown in Figure 4.

The parameter q_1 governs the process noise weighting for state variable x_1. Figure 4 Estimation results of different q_1 at 0.07–0.08 s demonstrates that increasing q_1 enhances tracking responsiveness at the expense of noise attenuation. Consequently, q_1 = 1 is selected to balance this.

Then the influence of q_3 on the filtering performance is researched. Here, $\boldsymbol{R}$ = 40, q_1 = 1 and q_2 = 0.01 in matrix $\boldsymbol{Q}$ were invariable, and the instantaneous speed estimation results when q_3 = 1, 10, 20 were selected respectively were shown in Figure 5.

As shown in Figure 5, the convergence speed of the speed is accelerated along with the increase of q_3. Since q_3 from 1 to 10 has almost no effect on the results, so q_3 is selected as 1. Finally, $\boldsymbol{Q}$ = diag(1, 0.01, 1) is selected as the optimal process noise covariance matrix.

To compare the filtering effect and verify the restoration degree of the original signal, signal to noise ratio (SNR) and consistency estimation r^2 are introduced as evaluation indicators:

$$\mathrm{SNR} = 10\lg\frac{P_s}{P_n} = \frac{\sum_{k=1}^{N} y(k)^2 \Big/ N}{\sum_{k=1}^{N} n(k)^2 \Big/ N} \tag{31}$$

$$r^2 = 1 - \frac{\sum_{k=1}^{N}\left|y_0(k) - \hat{y}(k)^{+}\right|^2}{\sum_{k=1}^{N}\left|y_0(k) - \bar{y}(k)\right|^2} \tag{32}$$

where N is the length of the signal, P_s is the signal power, P_n is the noise power, and $y(k)$ is the instantaneous speed at the k instant.

The performance of the EKF heavily depends on the appropriate selection of the noise covariance matrices. To ensure robust estimation, a sensitivity analysis is conducted by varying the diagonal elements of $\boldsymbol{Q}$ and the scalar $\boldsymbol{R}$. The influence of different parameter choices on tracking accuracy and noise suppression is examined. In summary, by comparing results with different $\boldsymbol{Q}$, $\boldsymbol{R}$ and considering both the filtering effect and convergence speed, $\boldsymbol{Q}$ and $\boldsymbol{R}$ are finally selected as:

Table 1 The performance of EKF under different parameters

q_1	q_2	q_3	$\boldsymbol{R}$	SNR(y)	SNR($\hat{y}$)	R^2
0.1	0.01	10	30	22.54	28.23	0.9992
0.1	0.01	10	40	22.54	28.89	0.9989
0.1	0.01	10	50	22.54	29.43	0.9987
0.1	0.01	10	40	22.54	28.89	0.9989
1	0.01	10	40	22.54	28.55	0.9993
10	0.01	10	40	22.54	27.10	0.9996
1	0.01	0.1	40	22.54	34.28	0.9928
1	0.01	1	40	22.54	32.47	0.9983
1	0.01	10	40	22.54	28.55	0.9993

$$\boldsymbol{Q} = \operatorname{diag}(1, 0.01, 1), \boldsymbol{R} = 40 \tag{33}$$

4.3 Estimation of simulation signal based on EKF

Based on the equation (28), the initial value of the state variable $\boldsymbol{x}(0)^+$ is set to [20 20 900], and the initial value of the prior estimate covariance matrix $\boldsymbol{P}(0)^+$ is set to diag([1 1 1]). Using the covariance matrices determined in equation (33), the method proposed in this paper is applied to estimate simulation signal defined by the equation (32).

As shown in Figure 6, the EKF estimated signal is in good agreement with the noise-free signal, confirming effective noise suppression. During 0.20–0.24 seconds, the estimated signal has a very high degree of reduction to the periodic fluctuation of the noise-free signal, validating the EKF's real-time filtering ability for instantaneous speed signals.

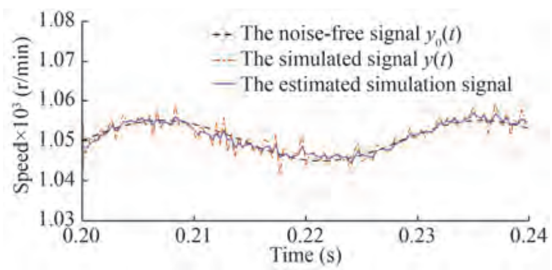

Figure 6 Comparison of instantaneous speed simulation results

In addition, the SNR of the actual signal and the estimated speed is SNR(y) = 22.5394 and SNR($\hat{y}$) = 32.4672, respectively. The consistency estimation between the real signal y_0 and the estimated speed $\hat{y}$ is $r^2 = 0.9983$, confirming exceptional waveform fidelity. These metrics demonstrate substantial noise attenuation while preserving critical speed dynamics. In summary, the design of the EKF realizes the real-time fast tracking of the instantaneous speed signal and successfully filters the noise.

5 Experiment and result analysis

5.1 Test bench introduction and data acquisition

To validate the effectiveness of the extended Kalman filter, the D4114 supercharged and intercooled marine diesel engine test bench is taken as the research object, as shown in Figure 7. The test bench mainly integrates four critical parts: the marine diesel engine, the hydraulic dynamometer, the cooling system, and the diesel engine control cabinet. The main parameters of D4114 marine diesel engine are shown in Table 2.

Figure 7 Test bench of D4114 marine diesel engine

Table 2 Main parameters of D4114 marine diesel engine

The name of parameters	value
Number of cylinders	4
Ignition order	1-3-4-2
Cylinder diameter (mm)	114
Piston stroke (mm)	135
Compression ratio	17.3:1
Rated power (kw)	90
Idling speed (r/min)	700
Rated speed (r/min)	1500

Test speed and load conditions are set through the control cabinet. Data acquisition covered eight operational conditions: 900 r/min, 0 kw; 900 r/min, 10 kw; 900 r/min, 20 kw; 1 000 r/min, 0 kw; 1 000 r/min, 10 kw; 1 000 r/min, 20 kw; 1 500 r/min, 40 kw; 1 500 r/min, 50 kw. The operation conditions cover typical marine operating profiles while excluding full-load scenarios due to test bench constraints. The data acquisition system is composed of the photoelectric encoder, signal conditioning board, NI-4432 acquisition card and computer. Before data acquisition, the sensor needs to be calibrated. Firstly, the speed signal is collected under idling speed and no-load conditions, and the standard deviation of the instantaneous speed is determined to be less than 2 r/min, which is consistent with the theoretical fluctuation range. After that, the data will be collected under the stable operation conditions mentioned above. The instantaneous speed pulse signal is generated by the photoelectric encoder, converted into electrical signal by the signal conditioning board and digitized by the NI-4432 card. And the instantaneous speed signal is collected and stored by LabVIEW software in the computer. The specific working principle is shown in Figure 8.

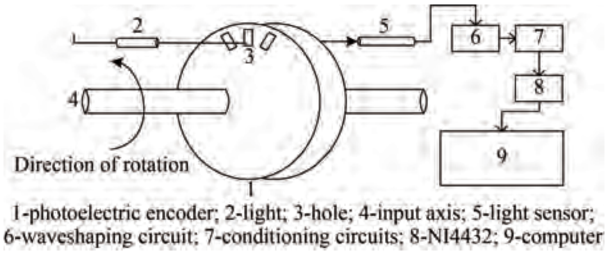

Figure 8 Working principle of speed signal acquisition

5.2 Pretreatment of instantaneous speed of diesel engine

The raw signal measured is the rotation time intervals $\Delta T(\Delta\theta_i)$ for each fixed angular increments $\Delta\theta$, where $\Delta\theta$ is determined by the hole number of photoelectric encoders. In this paper, the hole number Ne is 360, then $\Delta\theta = 360/Ne = 1°$. And the instantaneous speed is calculated as:

$$x(\Delta\theta_i) = \frac{60}{Ne \times T(\Delta\theta_i)} \tag{34}$$

For EKF compatibility, it is necessary to convert the speed at equal angular intervals into equal time intervals. Firstly, a non-uniform time axis τ_i is constructed through cumulative integration of rotation times:

$$\tau_i = \sum_{i=1}^{I} \Delta T(\Delta\theta_i) \quad i = 1, 2, \cdots, I \tag{35}$$

where τ_i denotes the absolute timestamp of the angular sample θ_i.

Then, the dataset $(\tau_i, x(\Delta\theta_i))$ is resampled to equal time-intervals using cubic spline interpolation. In this paper, F_S is set as 12800 Hz, and equal time-interval $\Delta t = 7.8125\times10^5$s.

Figure 9(a) displays signal with equal-angle interval at 900 r/min 10 kW, while Figure 9(b) shows the corresponding resampled equal-time signal.

As shown in Figure 9(a) and Figure 9(b), the instantaneous speed has the influence of noise such as burrs. To suppress the disturbance while preserving true signals, the proposed EKF is applied to the signal with equal time interval.

5.3 The instantaneous speed is estimated based on EKF

The key parameters for state-space can be obtained by analyzing the instantaneous speed signal in Figure 9. It can

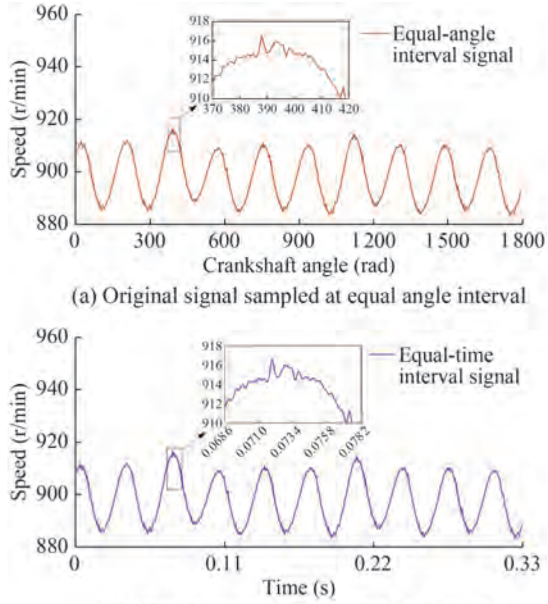

(a) Original signal sampled at equal angle interval

(b) Signal resampled at equal time interval

Figure 9 Signal at equal-angle interval and equal-time interval

be calculated that the average speed $\bar{x}$ = 898.36 r/min, and the fluctuation amplitude a is 16.30 r/min. The coefficient b is 0.209 4. The sampling rate F_S is set as 12 800 Hz and the sampling interval $\Delta t = F_S = 7.8125\times10^{-5}$ s. To sum up, equation (7) can be rewritten as follows:

$$\begin{cases} \dot{\boldsymbol{x}} = \begin{bmatrix} \dot{x}_1 \\ \dot{x}_2 \\ \dot{x}_3 \end{bmatrix} = \begin{bmatrix} 16.30 \times \omega\cos(\omega t) \\ -16.30 \times \omega\sin(\omega t) \\ 0 \end{bmatrix} = \begin{bmatrix} 0.209\,4 \cdot x_3 \cdot x_2 \\ -0.209\,4 \cdot x_3 \cdot x_1 \\ 0 \end{bmatrix} \\ \boldsymbol{y} = \begin{bmatrix} 1 & 0 & 1 \end{bmatrix} \begin{bmatrix} x_1 \\ x_2 \\ x_3 \end{bmatrix} \end{cases} \tag{36}$$

The initial state variable and the noise covariance matrix are set as: $\boldsymbol{x}(0)^+ = [x_1(0)^+ \; x_2(0)^+ \; x_3(0)^+] = [16.30 \;\; 16.30 \;\; 898.036]$, $\boldsymbol{P}(0)^+ = \mathrm{diag}([1 \;\; 1 \;\; 1])$. And the noise covariance matrix $\boldsymbol{Q}$ and $\boldsymbol{R}$ are set as the equation (33). Following EKF implementation, and the comparison between the actual instantaneous speed and the estimated instantaneous speed is shown in Figure 10.

As shown in Figure 10(a), the proposed EKF accurately tracks the instantaneous speed fluctuations while effectively suppressing background noise. Figure 10(b) provides a detailed view demonstrating that burrs and other noise in the measured signal are effectively eliminate, enabling accurate estimation of the instantaneous speed of the marine diesel engine.

The test data of 10 groups in each of 8 test conditions were selected as samples. The samples are processed using the EKF, and the SNR of the instantaneous speed before and after estimation is calculated. The comparison of the SNR for 10 groups of samples under each operating condition is shown in Figure 11.

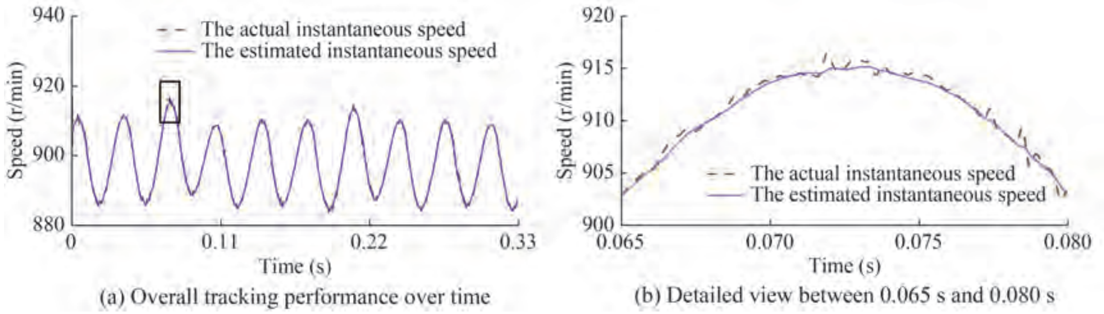

Figure 10 Comparison of estimation results at 900 r/min 10 kw

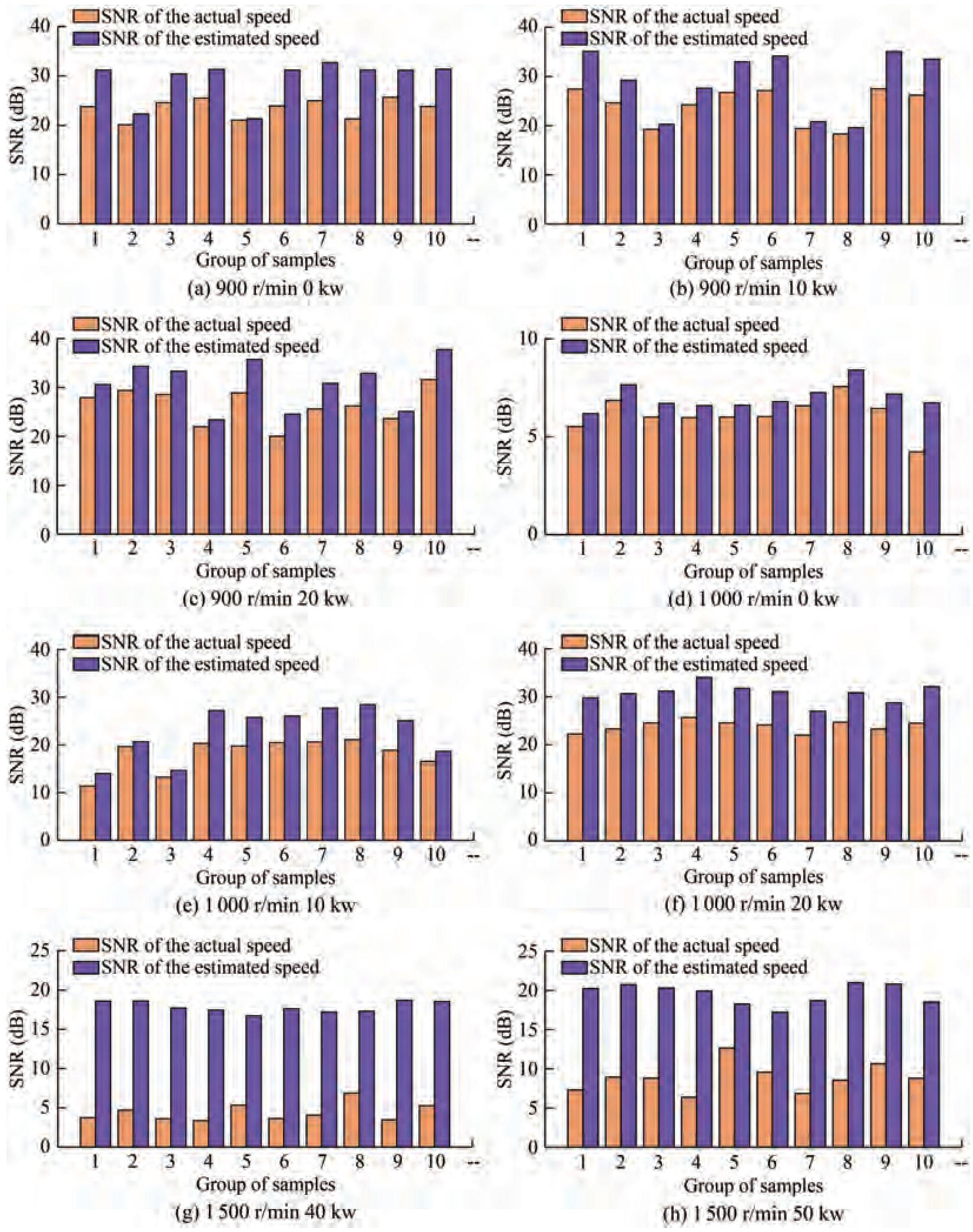

Figure 11 Comparison of the SNR of 10 groups of samples under each operating condition

Table 3 presents the average SNR of the actual speed and estimated speed across 10 groups of samples and SNR improvement rate under each operating condition. The SNR improvement rate is calculated using equation (37):

$$\varDelta = \frac{\mathrm{SNR}\left(\hat{y}\right) - \mathrm{SNR}\left(y\right)}{\mathrm{SNR}\left(\hat{y}\right)} \tag{37}$$

Table 3 The average SNR of 10 groups of samples and SNR improvement rate under each operating condition.

Operating condition	SNR(y)	SNR($\hat{y}$)	$\varDelta$/%
900 r/min, 00 kw	23.4703	29.4118	20.20
900 r/min, 10 kw	24.0907	28.8282	16.43
900 r/min, 20 kw	26.3839	30.8457	14.46
1000 r/min, 00 kw	6.1224	7.0122	12.69
1000 r/min, 10 kw	18.2106	22.8315	20.24
1000 r/min, 20 kw	23.9080	30.7208	22.18
1500 r/min, 40 kw	4.4109	17.8493	75.29
1500 r/min, 50 kw	8.8460	19.5614	54.78

As shown in Figure 11 and Table 3, the EKF-based estimation method exhibits significantly higher SNR than the measured instantaneous speed across all operating conditions, confirming the method's effectiveness.

Notably, the SNR improvement rate of 1500 r/min, 40 kw and 50 kw is 75.29% and 54.78% respectively. The main reason for this phenomenon is that the cylinder firing frequency increases under high-speed and high-load, and the high frequency noise of the instantaneous speed signal of the crankshaft is amplified. Consequently, the original signal exhibits a relatively low SNR of 4.4109 under the conditions. Furthermore, the low baseline SNR also contributes to the anomalously high improvement rates. In summary, the EKF designed in this study can estimate the signal in real time while effectively suppressing noise, thereby obtaining a more accurate instantaneous speed signal.

6 Conclusions

To address instantaneous speed fluctuation in marine diesel engines and achieve accurate real-time estimation, this paper proposes an EKF-based estimation method for instantaneous speed signals.

The principal conclusions are as follows:

Based on the fluctuation characteristics of the crankshaft instantaneous speed, a mathematical model representing instantaneous speed as the superposition of a sinusoidal signal and a constant term is established. A novel nonlinear state-space model is proposed, where the fluctuation of the instantaneous speed, the derivative of the fluctuation and the average rotational speed are taken as three state variables, and the observability of the model is verified using Lie derivative analysis.

An extended Kalman filter (EKF) is designed to enable real-time estimation through feedback correction using the residual between measured and estimated instantaneous speeds. Furthermore, the influence of different noise covariance matrix $\boldsymbol{Q}$ and $\boldsymbol{R}$ on the estimation performance is studied, and the optimal $\boldsymbol{Q}$ and $\boldsymbol{R}$ are determined according to the filtering effect. In this paper, $\boldsymbol{Q} = \mathrm{diag}(1, 0.01, 1)$, $\boldsymbol{R} = 40$.

The algorithm is validated using both simulated signals and experimental data from a 4-cylinder marine diesel engine. The results show that the consistency estimation between the estimated speed and the actual speed is $R^2 = 0.998\,3$ and the improvement rate SNR is more than 10%, which proves that the model is very effective for estimating the instantaneous speed. This confirms the model's efficacy for instantaneous speed estimation and its capability to filter noise for accurate extraction of engine operational signatures. While theoretically suitable for other multi-cylinder engines, further verification is necessary for other engines such as variable-cylinder engines.

Competing interests The authors have no competing interests to declare that are relevant to the content of this article.

References

Cao Y, Wang J, Shen W (2021) High-performance PMSM Self-tuning Speed Control System with A Low-order Adaptive Instantaneous Speed Estimator using A Low-cost Incremental Encoder. Asian Journal of Control: Affiliated with ACPA, the Asian Control Professors, Association 1870-1884. https://doi.org/10.1002/asjc.2346

Chang Y, Hu Y (2010) Monitoring and Fault Diagnosis System for the Diesel Engine Based on Instantaneous Speed. In: 2010 2nd International Conference on Computer and Automation Engineering (ICCAE). IEEE, Singapore, pp 774-778. https://doi.org/10.1109/ICCAE.2010.5451800

Kai C, Huang G, Sun J (2023) Implementation and Precision Analysis of Speed Measurement System for Marine Main Engine. Journal of Physics: Conference Series 2477(1): 012083. https://doi.org/10.1088/1742-6596/2477/1/012032

Kallenberger C, Hamedović H, Zoubir A (2007) Comparison of The Extended Kalman Filter and The Unscented Kalman Filter for Parameter Estimation in Combustion Engines. In: 2007 15th European Signal Processing Conference. IEEE 2424-2428

Kazienko D, Chybowski L (2020) Instantaneous Rotational Speed Algorithm for Locating Malfunctions in Marine Diesel Engines. Energies 13(6): 1396. https://doi.org/10.3390/en13061396

Lin R, Tan C, Ma L, Joseph M (2015) Condition Monitoring and Fault Diagnosis of Diesel Engines using Instantaneous Angular Speed Analysis. Proceedings of the Institution of Mechanical Engineers, Part C: Journal of Mechanical Engineering Science 229(2): 304-315. https://doi.org/10.1177/0954406214533253

Liu C, Su Y, Zhang C (2024) Design of Motion Attitude Measurement System and Correction Method in Semi-airborne Frequency Domain Electromagnetic Detection. IEEJ Transactions on Electrical and Electronic Engineering 19(6): 938-949. https://doi.org/10.1002/tee.24023

Liu Y, Li J, Gong L (2022) Measurement Error of the Instantaneous Speed A/D Sampling Way Influence Factors Analysis. Journal of mechanical design and manufacturing 69-72. https://doi.org/10.19356/j.cnki.1001-3997.2022.06.049. in Chinese

Meng K, Liu Q, Zhang Z (2023) Sensorless HSPMSM Control of An Improved SMC and EKF Based on Immune PSO. Applied Sciences 13(22): 12407. https://doi.org/10.3390/app132212407

Pan F, Zhang Y (2011) The Denoising Method for Transient Speed Signal of Diesel Engine. Advanced Materials Research 291-294: 2081-2084. https://doi.org/10.4028/www.scientific.net/AMR.291-294.2081

Qian Q, Ting Q, Min L (2022) Monitoring and Diagnosis of Complex Production Process Based on Free Energy of Gaussian–Bernoulli Restricted Boltzmann Machine. Journal of Iron and Steel Research International 30(5): 971-984. https://doi.org/10.1007/s42243-022-00867-4

Qiao X, Gu C (2019) Research on Wear Status of Diesel Engine Cylinder Based on BP Neural Network and Instantaneous Speed. Journal of Physics: Conference Series 1237(5): 052011. https://doi.org/10.1088/1742-6596/1237/5/052011

Quartullo R, Garulli A, Giannitrapani A (2023) In-cylinder Pressure Estimation from Rotational Speed Measurements via Extended Kalman Filter. Sensors 23(9): 4326. https://doi.org/10.3390/s23094326

Rana R, Gaur P, Agarwal V (2019) Tremor Estimation and Removal in Robot-assisted Surgery using Lie Groups and EKF. Robotica 37(11): 1904-1921. https://doi.org/10.1017/S0263574719000341

Wang L, Guan R (2022) State Feedback Control and Kalman filtering with MATLAB/Simulink Tutorials. IEEE Control Systems 1-416. https://doi.org/10.1002/9781119694625

Wu L, Fu Y, Li M, Liang G, Zhang Y, Cui Y (2021) The Effects of Material and Structure of Main Bearing Caps on Crankshaft Lubrication of Diesel Engine. International Journal of Engine Research. 22(4): 1086-1100. https://doi.org/10.1177/1468087419896647

Xi T, Cao R, Chen F (2016) Zoom Synchrosqueezing Transform for Instantaneous Speed Estimation of High Speed Spindle. Materials Science Forum 836-837: 310-317. https://doi.org/10.4028/www.scientific.net/MSF.836-837.310

Xie L, Sun S, Dong F (2023) The Non-uniformity Control Strategy of A Marine High-speed Diesel Engine Based on Each Cylinder's Exhaust Temperature. Processes 11(4): 1256. https://doi.org/10.3390/pr11041068

Yang K, Zhou L, Gong G (2018) Numerical Algorithms of Marine Diesel Engine Instantaneous Speed Based on Hilbert-Huang Transform. IOP Conference Series: Materials Science and Engineering 382: 052001. https://doi.org/10.1088/1757-899X/382/5/052017

Yu H, Duan S (2014) Crankshaft Transient Motion Analysis for Marine Diesel Engine. Advanced Materials Research 926-930: 773-776. https://doi.org/10.4028/www.scientific.net/AMR.926-930.773

Zerdali E (2019) Adaptive Extended Kalman Filter for Speed-sensorless Control of Induction Motors. IEEE Transactions on Energy Conversion 34(2): 789-800. https://doi.org/10.1109/TEC.2018.2866383

Zhao J, Chen L (2019) Research on Optimization Method of Instantaneous Speed State Characteristics of Diesel Engine Based on Genetic Algorithm. In: The 2019 International Conference on Artificial Intelligence and Computer Science (AICS 2019). ACM, New York, NY, USA, pp 394-398. https://doi.org/10.1145/3358331.3358365

Zhao M, Lin J, Liao Y (2015) Instantaneous Rotating Speed Estimation using Adaptive Short-time Chirp-Fourier Transform and its Applications. Journal of Mechanical Engineering 51(14): 8-14. https://doi.org/10.3901/JME.2015.14.008

Zhang M, Zi Y, Niu L (2019) Intelligent Diagnosis of V-type Marine Diesel Engines Based on Multifeatures Extracted from Instantaneous Crankshaft Speed. IEEE Transactions on Instrumentation and Measurement 68(3): 722-740. https://doi.org/10.1109/TIM.2018.2857018

Zheng T, Yan L, Yi D (2017) Angle Conversion Method of Diesel Engine Based on Instantaneous Speed Signal. Journal of Beijing University of Chemical Technology (Natural Science Edition) 44 (6): 70-75. https://doi.org/10.13543/j.bhxbzr.2017.06.011